A ROI-based global motion model established on 4DCT and 2D cine-MRI data for MRI-guidance in radiation therapy

Noemi Garau[1], Riccardo Via[1,*], Giorgia Meschini[1], Danny Lee[2], Paul Keall[3], Marco Riboldi[4], Guido Baroni[1,5] and Chiara Paganelli[1].

[1]*Dipartimento di Elettronica, Informazione e Bioingegneria, Politecnico di Milano, Milano, Italy*
[2] *Department of Radiation Oncology, Calvary Mater Newcastle, Newcastle, New South Wales, Australia*
[3] *ACRF Image X Institute, Sydney Medical School, University of Sydney, Sydney, New South Wales, Australia*
[4]*Chair of Experimental Physics - Medical Physics, Ludwig-Maximilians-Universität München, Munich, Germany*
[5]*Bioengineering Unit, CNAO Foundation, Pavia, Italy*

Abstract

In-room Magnetic Resonance Imaging (MRI) allows the acquisition of fast 2D cine-MRI centered in the tumor for advanced motion management in radiotherapy. To achieve 3D information during treatment, patient-specific motion models can be considered the most viable solution. However, conventional global motion models are built using a single motion surrogate, independently from the anatomical location.

In this work, we present a novel motion model based on regions of interest (ROIs) established on 4D Computed Tomography (4DCT) and 2D cine-MRI, aiming at accurately compensating for changes during treatment. In the planning phase, a motion model is built on a 4DCT dataset, through 3D deformable image registration (DIR). ROIs are then defined and correlated with motion fields derived by 2D DIR between CT slices centered in the tumor. In the treatment phase, the model is applied to in-room cine-MRI data to compensate for organ motion in a multi-modal framework, aiming at estimating a time-resolved 3DCT.

The method is validated on a digital phantom and tested on two lung patients. Analysis is performed by considering different anatomical planes (coronal, sagittal and a combination of the two) and evaluating the performance of the method on tumor and diaphragm. For the phantom study, the ROI-based model results in a uniform median error on both diaphragm and tumor below 1.5mm. For what concerns patients, median errors on both diaphragm and tumor are around 2mm (maximum patient resolution), confirming the capability of the method to regionally compensate for motion.

A novel ROI-based motion model is proposed as an integral part of an envisioned clinical MRI-guided workflow aiming at enhanced image guidance compared to conventional strategies.

1. Introduction

In recent years, the advent of in-room Magnetic Resonance Imaging (MRI) systems integrating MRI scanners with delivery units (i.e. MRI-linacs), paved the way to innovative image-guided solutions in radiation therapy (Menard *and* van der Heide 2014, Paganelli *et al.* 2018). Routine clinical application of such systems is expected

[*]*Current address: Center for Proton Therapy, Paul Scherrer Institut, CH-5232 Villigen PSI, Switzerland*

to reduce target localization errors, with improved target coverage and sparing of surrounding healthy tissues (Jaffray 2012). The treatment of mobile tumors, i.e. lesions affected by respiratory motion, will especially benefit from these technologies, which enables non-ionizing anatomical in-room imaging combined with advanced motion management strategies (Keal *et al.* 2006b; Colvill *et al.* 2016).

In current in-room MRI systems (Fallone 2014; Keall 2014; Jaffray 2012; Langendijk 2014; Mutic 2014), the trade-off between acquisition time and image quality suggests fast 2D cine-MRI centered in the tumor as the preferred imaging solution for motion detection, thus providing internal anatomy information at a good temporal resolution. Different solutions for gating (Park *et al.* 2016) or tumor tracking (Fast *et al.* 2017) based on this technique have already been proposed: template matching (Cervino *et al.* 2011; Shi *et al.* 2014; Tryggestad *et al.* 2013a), landmark tracking (Paganelli *et al.* 2015; Seregni *et al.* 2016; Mazur *et al.* 2016) and 2D deformable image registration (DIR) (Seregni *et al.* 2018) methods are the most explored target referencing strategies in the literature (Menten *et al.* 2017; Fast *et al.* 2017). However, the bi-dimensional information provided by the cine-MRI approach does not fully characterize the 3D motion of the whole tumor, making it difficult to accurately compensate for motion of irregularly shaped or deformable tumors. A practical countermeasure is based on the MRI capability to allow image acquisition along different orientations, thus enabling fast interleaved orthogonal cine-MRI slices intersecting the target and reconstructing the 3D position of the tumor (Sawant *et al.* 2014; Bjerre *et al.* 2013). This however is limited to the local information centered in the tumor. Another viable solution is therefore represented by patient-specific global motion models, which relate in-room surrogates with time-resolved pre-treatment imaging and enables reconstructing the whole 3D anatomy during treatment (McClelland *et al.* 2013). This is particularly suitable for multi-target tracking problems, such as lung cancer, where both the primary tumor and involved nodes need to be simultaneously targeted, and for retrospective calculation of the accumulated dose in both tumor and organs at risk (Kamerling *et al.* 2016).

Conventional global motion models for image-guided radiotherapy, are built on four-dimensional Computed Tomography (4DCT), being the current clinical standard of time-resolved imaging for treatment planning (Keall 2004). These models rely on the correlation of deformation vector fields derived from 3D DIR between 4DCT respiratory phases with a mono-dimensional external surrogate. A recent study investigated the performance of a motion model using external and internal surrogates. Better results were achieved using lung volume as a surrogate, suggesting the use of internal structures as the most advantageous solution (Wölfelschneider *et al.* 2017).

In the MRI-guidance scenario, 4DMRI scans can be acquired as pre-treatment images both prospectively (Hu *et al.* 2013) or retrospectively (Paganelli *et al.* 2015; Von Siebenthal *et al.* 2007; Deng *et al.* 2016), with improved soft tissue contrast and the advantage of radiation sparing to the patient with respect to 4DCT. However, the lack of electron density information prevents dosimetric quantification. Currently, 4DMRI has been already explored as on-board imaging for motion model construction with navigator slices (Fayad *et al.* 2012) or 2D cine-MRI data (Harris *et al.* 2016; Stemkens *et al.* 2016, de Seneville *et al*. 2015) being used to obtain in-room motion information. A recent work investigated also the effect of inter and intra-fractional motion in kidney, by means of an on-board (pre-beam) 4DMRI motion model and simulated pseudo CT (Stemkens *et al.* 2017).

A potential limitation of these approaches for motion modeling relies on the assumption of a correlation between the one-dimensional in-room motion and the

changing anatomy, independently from the anatomical location. Fayad *et al.* (2012) used the diaphragm position in the navigator as a single motion trace, while Harris *et al.* (2016) and Stemkens *et al.* (2016) derived a weighting factor from a similarity metric between pre-treatment images and 2D cine-MRI for the adaptation over the entire anatomy. Additionally, none of these MRI-guided motion models were directly built nor included information on a pre-treatment 4DCT, thus limiting potential clinical applicability related to an optimized dosimetric plan directly defined on 4DCT.

In this work, we propose a novel global motion model aiming at accurately compensating for motion of anatomo-pathological structures in the framework of lung MRI-guided radiation therapy. The model is based on regions of interest (ROIs) to differentiate between anatomical districts and, therefore, mitigate the effect of uneven respiratory motion. This approach is put forward as part of an envisioned clinical workflow where the potential of multi-modal imaging is exploited. Specifically, the motion model is built on a planning 4DCT dataset and applied to in-room 2D cine-MRI data. This could be potentially used in a clinical scenario to accurately account for motion and perform dosimetric evaluations, relying on current standards for motion management provided by the 4DCT dataset.

The proposed workflow was simulated with a digital CT/MRI lung phantom for validation purposes. In addition, a preliminary application on two lung patients is reported.

2. Material and Methods

In this section, we present an outline of the methodological solution developed for the ROI-based motion model using planning 4DCT, pre-beam 3D T1-weighted MRI and in-beam interleaved 2D sagittal and coronal cine-MRI data. The ROI-based motion model allows the volumetric estimation of a time-resolved virtual 3DCT of the internal patient configuration. The performance of the proposed approach is evaluated on a dataset comprising synthetic and clinical data.

2.1. ROI-based motion model

The workflow of the method can be divided in two main steps: model construction and model application. During the construction process, we derive a model which couples the 3D motion, derived from 4DCT data, with 2D motion, derived from 2D CT slices centred in the tumor. A principal component analysis (PCA) approach (Fayad *et al.* 2012) is implemented for model creation on ROIs related to anatomical structures. To assure 2D slice correspondence between planning and in-beam acquisition needed for model application, a 3D rigid registration is performed between the planning 3D CT and a pre-beam 3D MRI. The model is then applied relying on in-beam 2D motion information, derived by generating virtual 2D cine-CT images from acquired 2D cine-MRI, in a multi-modal registration pipeline. This aims at estimating the 3D anatomical deformation for each cine-MRI sample, deriving time-resolved 3DCT volumes.

The workflow of the proposed method is shown in Figure 1. Table 1 summarizes the set of images involved in the presented method and defines the terminology used in the following two sub-sections, where more details are given about model construction and model application procedures.

2.1.1. Model construction

The model construction is performed as follows.

i. 3D DIR on planning 4DCT

Respiratory motion is described as 3D non-rigid transformation with respect to the end-exhale reference volume, which is typically considered as the most stable respiratory phase. Specifically, 3D DIR is performed between each 4DCT phase and the reference exhale volume (3DCT-0%), to derive time-resolved 3D vector fields (3DVFs) representing organ motion during respiration. The registration consists of a 3D multi-stage mono-modal B-spline registration.

ii. Mono-modal 2D DIR

The model construction includes also the definition of respiratory motion information derived from 2D planning images. This is based on 2DVFs computed by means of 2D mono-modal DIR between orthogonal (coronal and sagittal) slices centred in the tumor at different respiratory phases of the 4DCT (sliceCT). Again, the exhale is considered as the reference for 2D DIR (sliceCT-0%). A single-stage 2D mono-modal B-spline registration is applied.

iii. ROI and 2D motion definition

ROIs are defined according to the available planning contours. Specifically, tumor and diaphragm are considered as main structures. These are used to divide the 3DVFs in the cranio-caudal direction, deriving an upper and a lower region which encompass the tumor and the diaphragm, respectively. Contours are also used to determine motion from the 2DVFs derived in (ii). In fact for each structure, the 2D motion information is derived by selecting the maximum value within the contour mask of

- right-left (RL) 2DVF component from coronal ($max2Dvf_1$),
- anterior-posterior (AP) 2DVF component from sagittal ($max2Dvf_2$),
- superior-inferior (SI) 2DVF component from both coronal and sagittal ($max2Dvf_3$).

iv. Model generation

To derive the ROI-based motion model, principal component analysis (PCA) is applied to the discretised 3DVFs and the 2DVFs maximum values, following the approach proposed by Fayad *et al.* (2009, 2012) (supplementary materials A).

For a respiratory phase in a specific ROI, the 3DVF and maximum values of 2DVF are placed in a vector:

$$d_{j\_ROI} = [3Dvf_{1,1,j}\ 3Dvf_{1,2,j}\ 3Dvf_{1,3,j}\ , \dots, 3Dvf_{m,i,j}, \dots, 3Dvf_{M,i,j}, \\ max2Dvf_{1,j}, max2Dvf_{2,j}\ , max2Dvf_{3,j}\ ]^T_{ROI_{planning}} \quad (1)$$

where, the $3Dvf_{m,i,j}$ is the i^{th} component of the 3DVF for the voxel m (with $0 < m \leq M$) at the respiratory phase j ($0 < j < J$) where J is the number of 3DVFs ($J = 9$), $i = 1,2,3$ for the RL, AP, SI displacement respectively, M is the total number of voxels, and $max2Dvf_{1,j}, max2Dvf_{2,j}\ , max2Dvf_{3,j}$ are the maximum values of 2DVF along RL, AP and SI respectively.

Then a matrix D_{ROI} is constructed as follows:

$$D_{ROI} = [d_{1_{ROI}}, d_{2_{ROI}}, \dots, d_{j\_ROI}, \dots, d_{J\_ROI}\ ] \quad (2)$$

with dimension $(3M + 3) * J$.
By applying PCA as in Fayad *et al.* (2009, 2012) along the first principal component, the eigenvalues and eigenvectors E of the covariance matrix $D_{ROI}D_{ROI}^{T}$ are computed. E is composed by the upper $3M$ rows ($E_{3Dvf_{ROI}}$) and the lower 3 rows ($E_{max2Dvf_{ROI}}$), allowing to derive the motion model B_{ROI} as follows:

$$B_{ROI} = E_{3Dvf_{ROI}}E_{max2Dvf_{ROI}}^{-1} \quad (3)$$

2.1.2. Model application

The model is then applied according to these following steps.

i. Pre-beam 3D registration

A volumetric rigid registration between a pre-beam 3D MRI acquired at the exhale (3DMRI-0%) and the planning 3DCT-0% is applied to achieve correspondence among 2D CT slices used during model construction and in-room acquisitions. This is performed under the assumption that no deformation occurred between planning and treatment, thus assuming a timely acquisition between CT and MRI data. This procedure is furtherly justified for the patient study, as 3D MRI scans were acquired under breath-hold condition, which does not represent the free-breathing exhale state (additional details in 4.1).

ii. In-beam multi-modal 2D DIR

Two stages of multi-modal 2D DIR are performed in this step (B-spline registration with mutual information as similarity metric).
At first, DIR is applied between in-beam cine-MRI data and corresponding 3DMRI-0% slices (sliceMRI-0%) selected through image alignment, to obtain a virtual T1-weighted cine-MRI (vcine-T1). Then, the resulting vcine-T1 is registered with 3DCT-0% corresponding slices (sliceCT-0%), generating a virtual cine-CT (vcine-CT).
The first stage is introduced to guarantee slice correspondence and to improve the performance of 2D DIR between sliceCT-0% and cine-MRI, whereas the second assures consistency between model construction (built on CT data) and model application.

iii. In-beam 2D motion definition

In-beam motion is defined by the selection of the maximum or minimum value of the in-beam 2DVFs (defined on vcine-CT) within the tumor and diaphragm masks. Here, differently from model construction, also minimum values of 2DVFs are taken into account, in order to compensate for baseline drifts consisting in a deeper exhale of the in-beam sample with respect to the reference sliceCT-0%. As such, by selecting the maximum value, positive motion variations with respect to the sliceCT-0% are compensated, whereas, by using the minimum, variations in the opposite direction can be managed. To define when to use the maximum or minimum value, contours delineated on the sliceCT-0% are warped on cine-MRI by applying the generated 2DVF: if the position of the warped contour is above the sliceCT-0% contour (deep-exhale), the minimum is selected; on the contrary (deep-inhale), the maximum is considered.

iv. Time-resolved virtual 3DCT estimation

To provide the estimated 3D deformation between the reference 3DCT-0% and the patient state as seen on cine-MRI, in-beam 2D motion values are fed to the ROI-based motion model for each ROI, as follows:

- in case of in-beam maximum value of the 2DVF

$$new3Dvf_{ROI} = B_{ROI} * [max2Dvf_1, max2Dvf_2, max2Dvf_3]_{ROI_{in\_beam}}$$

- in case of in-beam minimum value of the 2DVF

$$new3Dvf_{ROI} = B_{ROI} * [min2Dvf_1, min2Dvf_2, min2Dvf_3]_{ROI_{in\_beam}}$$

By merging the 3DVFs of the considered ROIs, a $new3Dvf$ is obtained describing the whole anatomy deformation. The inverted $new3Dvf$ is finally applied to deform the 3DCT-0% through volume warping, deriving a virtual 3DCT for each cine-MRI sample. The result is thus a time-resolved v3DCT.

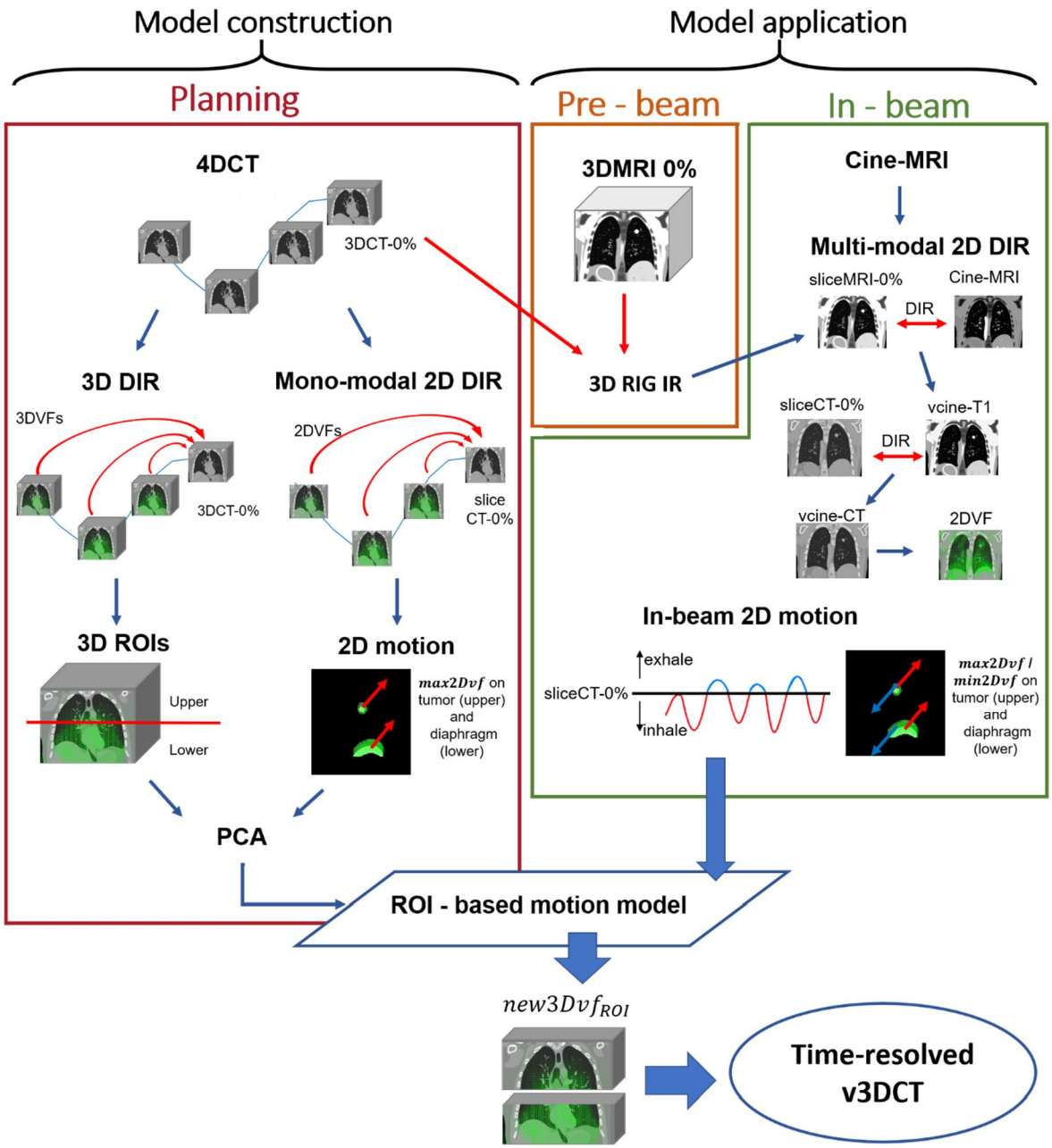

Figure 1. Schematic representation of the ROI-based motion model.

Table 1. Summary and terminology definition of images involved in the ROI-based motion model workflow.

Image set	Dimensionality	Time of acquisition	Use
4DCT	4D	Planning	4D image used to generate 3DVFs trough 3D DIR with respect to the exhale respiratory phase (3DCT-0%)
3DCT-0%	3D	Planning (end-exhale phase in 4DCT)	3D image used as reference in the 3D DIR process
sliceCT	2D	Planning	Set of coronal and sagittal slices centred in the tumor, selected from the 4DCT dataset. Used in the mono-modal 2D DIR process to generate 2DVFs to derive the maximum values of the 2DVF components.
sliceCT-0%	2D	Planning	Coronal and sagittal slices centred in the tumor, selected from the 3DCT-0%, used as reference in the mono-modal 2D DIR process.
3DMRI-0% (T1 weighted)	3D	Pre-beam	3D MR image (acquired at the exhale phase) involved in the 3D rigid registration process (3D RIG IR) to achieve correspondence between sliceCT and cine-MRI.
sliceMRI-0% (T1 weighted)	2D	Pre-beam	Coronal and sagittal slices centred in the tumor, selected from 3DMRI-0%, with same acquisition planes of in-beam cine-MRI. Used to support the 2D multi-modal DIR.
cine-MRI (T2/T1 weighted)	2D	In-beam	2D coronal/sagittal images involved in the multi-modal 2D DIR process to generate 2DVFs from which in-room maximum/minimum values of the 2DVF components are derived.
vcine-T1 (T1 weighted)	2D	In-beam	Virtual 2D coronal/sagittal T1-weighted images, which represent the output of the first stage of the multi-modal 2D DIR process.
vcine-CT	2D	In-beam	Virtual 2D coronal/sagittal CT images, which represent the output of the second stage of the multi-modal 2D DIR.
v3DCT	3D	In-beam	Output of the model: estimate of a virtual time-resolved 3DCT during irradiation.

2.2. Dataset

2.2.1. Phantom Data

The digital CT/MRI breathing anthropomorphic phantom (CoMBAT) introduced by Paganelli *et al.* (2017) was used to validate the proposed method. The phantom was animated using breathing signals acquired on a real patient (Lee *et al.* 2016). Simulated pre-treatment motion ranges were 9.6mm (SI) and 1.4/5.8mm (AP/SI) for diaphragm and tumor, respectively. In-room movements differed from planning of ±5mm for diaphragm and ±2mm for tumor; therefore, in-room motion ranges were about 15mm and 3/8mm.

4DCT volumes and T1-weighted 3D MRI were generated at a resolution of 384×384×256 with a voxel size of 1×1×1 mm. Cine-MRI data (384×256 pixels of 1×1×5 mm) were simulated with a frame rate of about 3 frames/s. MRI sequence parameters were derived from patient acquisitions and used to generate both T1-weighted MRI and T2-weighted cine-MRI.

2.2.2. Patient Data

Two lung cancer patients (P1, P2) were included in this study. 4DCT, pre-beam T1-weighted MRI scans and in-beam cine-MRI acquisition constitute the clinical dataset to simulate the real MRI-guided scenario (Table 2). However, one patient presented only coronal cine-MRI, as sagittal slices were not centred in the tumor at time of acquisition. For P2 both coronal and sagittal slices were correctly attained, though the latter exhibiting limited diaphragm visibility.

In the pre-treatment scenario, a motion of 13.3mm (SI) and 1.0/1.5mm (RL/SI) was measured in P1 for diaphragm and upper tumor, while differences from planning of in-room motion ranges were about ±9mm and ±0.7/±2.5mm, respectively.

For P2, diaphragm and tumor motion in planning phase was 17.7mm (SI) and 1.8/2.0/2.2mm (AP/RL/SI) respectively. In the in-room scenario, motion ranges differed from planning ones of ±3mm for diaphragm and ±1.1/±2.8/±2.5mm for tumor.

Table 2. Imaging parameters for clinical data.

Dataset	Imaging parameters
4DCT	10 respiratory phases size [pixels]: 515x512x84 (P01) 512x512x65 (P02) spacing [mm]: 0.78x0.78x2
3DMRI-0%	VIBE sequence TR/TE [ms]: 2.24/0.88 flip angle: 9° percent. sampling [%]:70 size [pixels]: 310x320x160 spacing [mm]: 1.18x1.18x1.2
Sagittal/coronal 2D cine-MRI*	TrueFISP sequence TR/TE [ms]= 3.03/1.32 flip angle: 45° percent. sampling: 65% accel. factor: 2 size [pixels]: 256x256 spacing [mm]: 1.48x1.48 slice thickness [mm]: 5

∗ Only coronal slices available for P1

2.3. Registration performance

To assess the accuracy of the mono-modal and multi-modal registrations used in the proposed study, we performed a quantitative evaluation for both phantom and patient data. Specifically, the analysis relied on quantifying the performance of (i) the 3D mono-modal DIR between CT volumes, (ii) the 2D mono-modal DIR between CT slices and (iii) the in-beam 2D multi-modal DIR computed to derive vcine-CT. Comparisons were performed between the 3DCT-0% (or sliceCT-0%) and the output of the registration for the mono-modal case, whereas the vcine-CT was compared with the cine-MRI for the multi-modal case. Tumor and diaphragm contours were warped accordingly and compared with the ground truth ones for DIR assessment. The metrics considered for DIR evaluation were as follows: the normalized mutual information (NMI) before and after registration on the upper and lower ROIs; the median distance of the diaphragm profile and the distance of the tumor center-of-mass (COM) after registration. For the 2D registrations, the quantification was performed on both sagittal and coronal samples.

2.4. Model performance

2.4.1. Phantom evaluation

The performance of the proposed ROI-based motion model was compared to the conventional motion model proposed by Fayad *et al.* (2012) (more details about Fayad model and its differences with the ROI-based model are reported in supplementary material A). The Fayad model was tested on the entire anatomy by using the diaphragm (Fayad-diaphragm) or the tumor (Fayad-tumor) motion as single motion trace.

Additionally, the performance of the proposed method was tested against the use of different anatomical planes during model construction and model application. Coronal and sagittal slices were considered separately using RL/SI (e.g. $max2Dvf_1/max2Dvf_3$ in ROI-based model) and AP/SI (e.g. $max2Dvf_2/max2Dvf_3$ in ROI-based model) components respectively. Also, a combination of two orientations was tested using the mean value of the SI components for coronal/sagittal combination.

Given the availability of ground truth volumes provided by the phantom, a quantitative volumetric analysis was possible between the estimated volumes and the ground truth volumes. Specifically, the distance between the diaphragm profile and the 3D distance of the tumor COM between time-resolved v3DCT and ground truth volumes were adopted as metrics of local discrepancy; whereas NMI was considered for a global evaluation in the upper and lower regions. The same quantifications were also performed between the ground truth volumes and the outputs of the Fayad model. A Friedman test (alpha=5%) was performed between error populations of diaphragm distance and COM, to define significant differences.

Moreover, the regularity of the $new3Dvf$ was evaluated by quantifying the difference of the estimated $new3Dvf$ with the one computed between the 3DCT-0% and the ground truth volume. This difference was assessed on the whole volume and at the interface (upper/lower ROIs) of the combined $new3Dvf$.

2.4.2. Patient evaluation

The proposed method was tested on clinical data where no ground truth was available. The analysis was therefore limited to 2D local comparison between in-room measurement (i.e. cine-MRI) and the corresponding slices of the estimated v3DCT. Specifically, tumor and diaphragm contours defined on the 3DCT-0% were warped on the cine-MRI and on the v3DCT data and compared. Structures displacement was evaluated in 2D along the available imaging plane.

A comparison with the Fayad model (supplementary material A) based on the sole diaphragm/tumor motion trace was also performed, as for the phantom study.

Additionally, a 3D comparison was performed between the estimated volume and the most similar respiratory phase in the 4DCT dataset, in order to account for variations between treatment and planning. The phase correspondence was defined by comparing cine-MRI and planning contours. NMI was calculated on the upper and lower ROIs and its correlation with structures displacement was evaluated using the Pearson's correlation coefficient (p-value = 5%).

For patient P2, the ROI-based motion model was applied on two different anatomical planes (coronal and sagittal separately) as well as on their combination. Only coronal plane was instead considered for patient P1, being the only one available.

The computational cost was also assessed for each step of the proposed workflow.

3. Results

3.1. Registration performance

Table 3 shows the performance of the mono-modal and multi-modal DIR used as a basis for the motion model construction during planning and subsequent in-beam application. NMI values increased after the registration in most of the cases for both the upper and lower regions. This was also accompanied by a median COM and diaphragm distance in the order of the voxel resolution for both mono-modal and multi-modal registration in phantom and patients' data.

Table 3. Median (IQR) errors of DIR performance. NMI values of the upper and lower regions are reported before / after DIR. Diaphragm and tumor COM distances are in [mm].

			Model construction			Model application	
			Mono-modal 3D DIR	Mono-modal 2D DIR		Multi-modal 2D DIR	
				sagittal	coronal	sagittal	Coronal
Phantom study	upper ROI	NMI (before/after)	1.11(0.07) / 1.31 (0.01)	1.12 (0.07) / 1.30 (0.02)	1.12 (0.07) / 1.35 (0.08)	1.7 (0.04) / 1.82 (0.01)	1.09 (0.08) / 1.45 (0.04)
		COM tumor distances	0.23 (0.22)	0.65 (0.31)	0.26 (0.19)	0.34 (0.36)	0.5 (0.55)
	lower ROI	NMI (before/after)	1.07 (0.06) / 1.24 (0.02)	1.18 (0.24) / 1.62 (0.03)	1.17 (0.21) / 1.67 (0.02)	1.59 (0.08) / 1.73 (0.00)	1.09 (0.14) / 1.37 (0.05)
		Diaphragm distances	0.09 (0.01)	0.0 (0.0)	0.0 (0.0)	0.0 (1.0)	1.0 (0.0)
P1	upper ROI	NMI (before/after)	1.15 (0.00) / 1.16 (0.00)		1.38 (0.02) / 1.39 (0.02)		1.23 (0.02) / 1.25 (0.02)
		COM tumor distances	0.0 (0.0)		0.43 (0.19)		0.07 (0.06)
	lower ROI	NMI (before/after)	1.14 (0.00) / 1.15(0.01)		1.41 (0.13) / 1.42 (0.01)		1.23 (0.11) / 1.24 (0.04)
		Diaphragm distances	1.09 (0.0)		1.0 (1.0)		0.0 (0.0)
P2	upper ROI	NMI (before/after)	1.15 (0.00) / 1.16 (0.00)	1.27 (0.01) / 1.28 (0.00)	1.25 (0.03) / 1.28 (0.02)	1.27 (0.01) / 1.28(0.05)	1.29 (0.01) / 1.30 (0.07)
		COM tumor distances	1.97 (3.02)	1.14 (0.47)	0.56 (0.51)	0.12 (0.08)	0.14 (0.11)
	lower ROI	NMI (before/after)	1.25 (0.07) / 1.28 (0.01)		1.30 (0.16) / 1.47(0.08)		1.30 (0.11) / 1.32 (1.37)
		Diaphragm distances	1.19 (0.008)		0.0 (0.0)		0.0 (0.0)

3.2. Model performance

3.2.1. Phantom study

Figure 2 summarizes the results of the quantitative comparison between the proposed method and the Fayad model in reconstructing the diaphragm and the tumor. When using the diaphragm/tumor motion signals for the Fayad model and combining the two available planes, we measured median errors of 1.71 mm (IQR: 2.13 mm) /1.86 mm (IQR: 2.77 mm) on the diaphragm, and 1.68 mm (IQR: 0.89 mm) / 1.27 mm (IQR: 0.77 mm) on the tumor. When the ROI-based approach is adopted, position was assessed with median errors of 1.04 mm (IQR: 0.92 mm), 0.83 mm (IQR: 0.75 mm), 0.82 mm (IQR: 0.66 mm) on diaphragm and 1.23 mm (IQR: 0.73 mm), 1.45 mm (IQR: 0.77 mm), 1.27 mm (IQR: 0.96 mm) on tumor, considering the sagittal, the coronal and the combination of both, respectively.

For diaphragm errors, significant differences were observed between ROI-based and Fayad-diaphragm and Fayad-tumor model; whereas for tumor errors, significant differences were obtained between ROI-based and Fayad-diaphragm in the sagittal/coronal combination. Figure 3 shows the qualitative performance of the ROI-based model with respect to the Fayad model.

Regarding NMI values on the upper and lower ROIs, no relevant variations were observed between the ROI-based and Fayad model. By combining the two planes, NMI median values in the upper and lower ROI were 1.49 (IQR: 0.05), 1.47 (IQR: 0.06) and 1.49 (IQR: 0.09) for the ROI-based, Fayad-diaphragm and Fayad-tumor, respectively.

The difference between the estimated VF ($new3Dvf$) and the one derived between 3DCT-0% and the ground truth volume (Figure 4) was in median 0.36 mm (IQR: 0.41 mm) for the whole volume and 0.29 mm (IQR: 0.54 mm) at the 3DVFs interface. Maximum errors (excluding the heart) were within ±2mm. Errors lower than -2mm were mainly quantified in the heart area (Figure 4b).

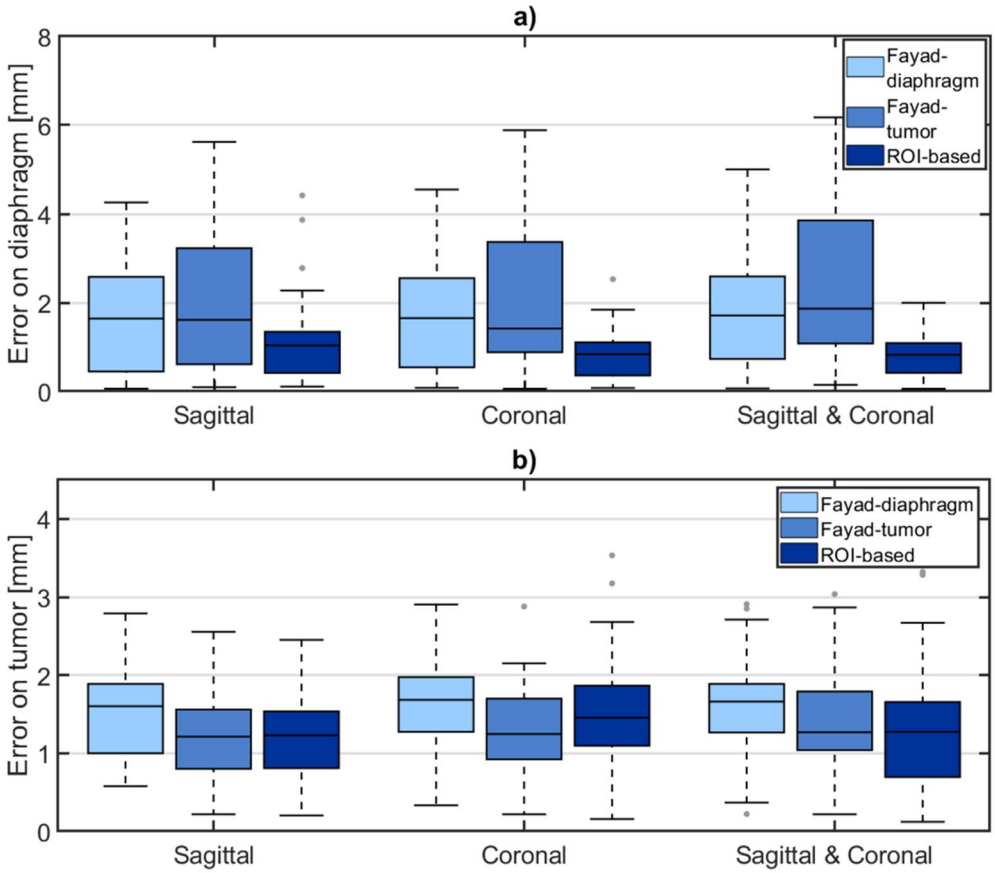

Figure 2. Phantom study – quantitative results. Errors on diaphragm (a) and tumor (b) as a function of anatomical planes for the ROI-based model and the Fayad model. This latter tested with diaphragm (Fayad-diaphragm) or tumor (Fayad-tumor) as single motion signal.

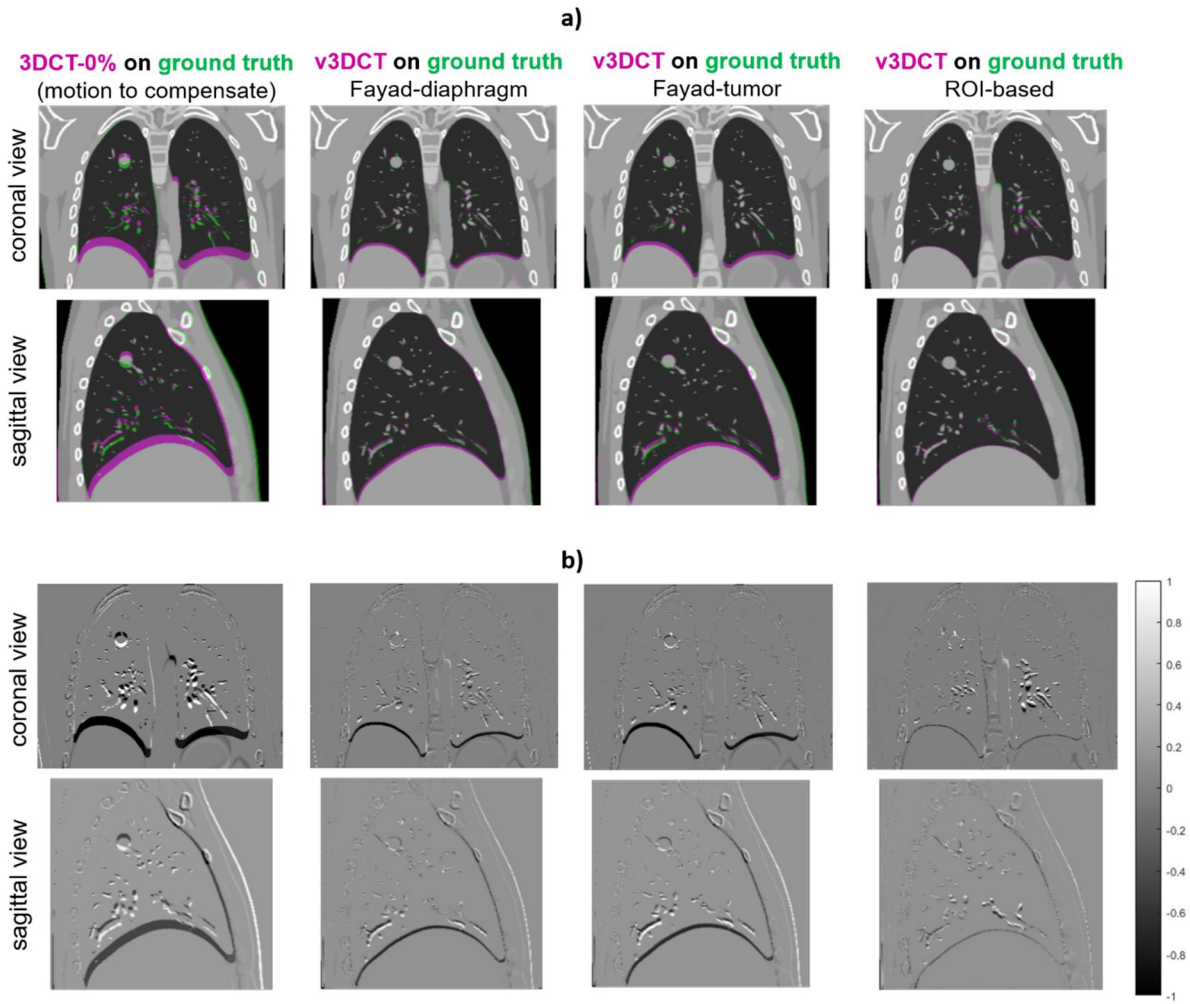

Figure 3. Phantom study – qualitative results. Panel (a) shows a comparison between the estimated v3DCT with the ROI-based motion model and the Fayad model (with diaphragm or tumor as motion signal): the estimated v3DCT (violet) is overlapped on the ground truth (green); the motion to compensate is illustrated by overlapping the 3DCT-0% (violet) on the ground truth (green). Panel (b) reports volume differences [-1,1] of the same image sample reported in (a).

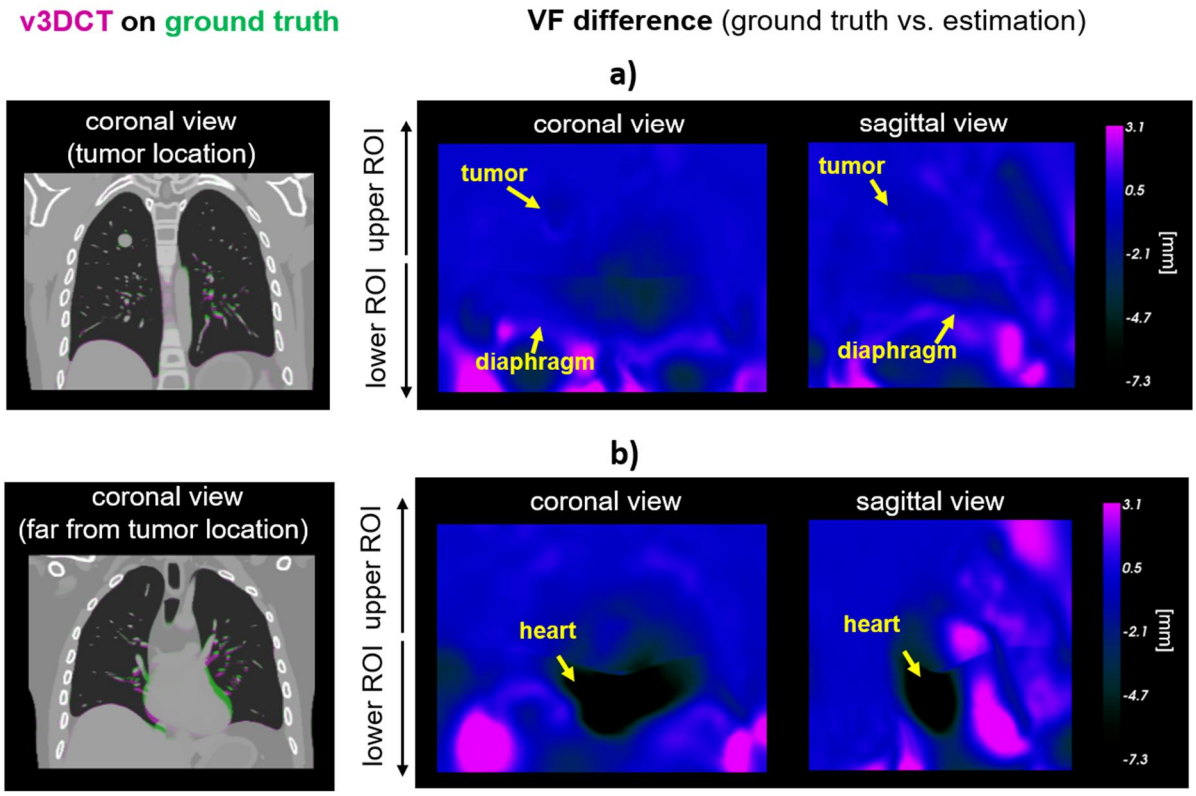

Figure 4. Phantom study – difference in mm between the estimated VF and the one derived between 3DCT-0% and the ground truth volume. Two different locations, related to the same respiratory phase as one in Figure 3, are reported: sagittal and coronal view centred in the tumor (a) and far from the tumor (b). Correspondent image overlap between v3DCT (violet) and ground truth (green) is reported on the left in the coronal view.

3.2.2. Patient study

The ROI-based method performance on clinical data depending on the considered anatomical plane is reported in Table 4. For P1, errors within 2 mm were found by considering the coronal slice only. For P2, the combination of coronal and sagittal slices resulted in a lower median error on the diaphragm compared to single planes. Errors above 2 mm were measured when considering the RL (coronal) direction, while lower errors were found in the AP/SI direction for all the investigated anatomical planes. The diaphragm profile and tumor COM trajectories as seen on cine-MRI and v3DCT corresponding slices are shown in Figure 5 for patient P1 and P2.

A similar trend as in the phantom study was observed also for patients when comparing the ROI-based motion model with the Fayad model based on the sole diaphragm/tumor motion signal. Specifically, for P1, errors on diaphragm were <1mm when using Fayad-diaphragm, but errors in SI of 2.10 mm (IQR: 2.97 mm) were observed on the tumor compared to 1.16 mm (IQR: 0.99 mm) quantified for the ROI-based model. The ROI-based model provided also lower errors than Fayad-tumor (3.5 mm (IQR: 7.0 mm) / 2.53 mm (IQR: 3.28mm) on diaphragm/tumor for Fayad-tumor). For P2, errors on diaphragm were comparable for ROI-based and Fayad model. Errors on tumor were instead quantified below 1 mm in the coronal direction by the Fayad model, but discrepancies up to 5 mm were found in the sagittal direction.

Regarding the difference between volumes of nearest phases in planning and treatment, for P1, NMI median values were 1.23 (IQR: 0.01) and 1.21 (IQR: 0.03) for upper and lower ROIs, respectively. Considering the combination of the two planes for P2, NMI median values of 1.29 (IQR: 0.12) / 1.35 (IQR: 0.07) were measured on upper/lower regions. A statistically significant correlation between distances of

associated phases and NMI values was found for the ROI including the diaphragm (Figure 6a). Conversely, a lower correlation was found for the upper region relevant to tumor (Figure 6b). A qualitative representation of the comparison between the estimated v3DCT and the identified nearest 3DCT of the average respiratory cycle is shown in Figure 6c.

Table 4. Discrepancies between diaphragm and tumor position of the cine-MRI and the corresponding slice of the estimated v3DCT for P1 and P2. SI, RL and AP refer to anatomical axes, i.e. superior-inferior, right-left and antero-posterior, respectively. Results are presented as median (IQR) and expressed in mm.

Patient	Structure	Coronal		Sagittal		Anatomical plane
		SI	RL	SI	AP	
P1	Diaphragm	2.22 (1.48)				Coronal
	Tumor	1.16 (0.99)	0.98 (0.49)			
P2	Diaphragm	2.22 (1.48)				Coronal
		2.96 (1.48)				Sagittal
		1.48 (2.96)				Cor & Sag
	Tumor	0.70 (1.07)	2.32 (3.82)	2.16 (1.06)	1.36 (1.81)	Coronal
		1.52 (2.46)	1.39 (2.08)	0.68 (0.81)	1.11 (1.39)	Sagittal
		1.35 (1.60)	1.69 (1.62)	1.01 (0.78)	0.88 (1.47)	Cor & Sag

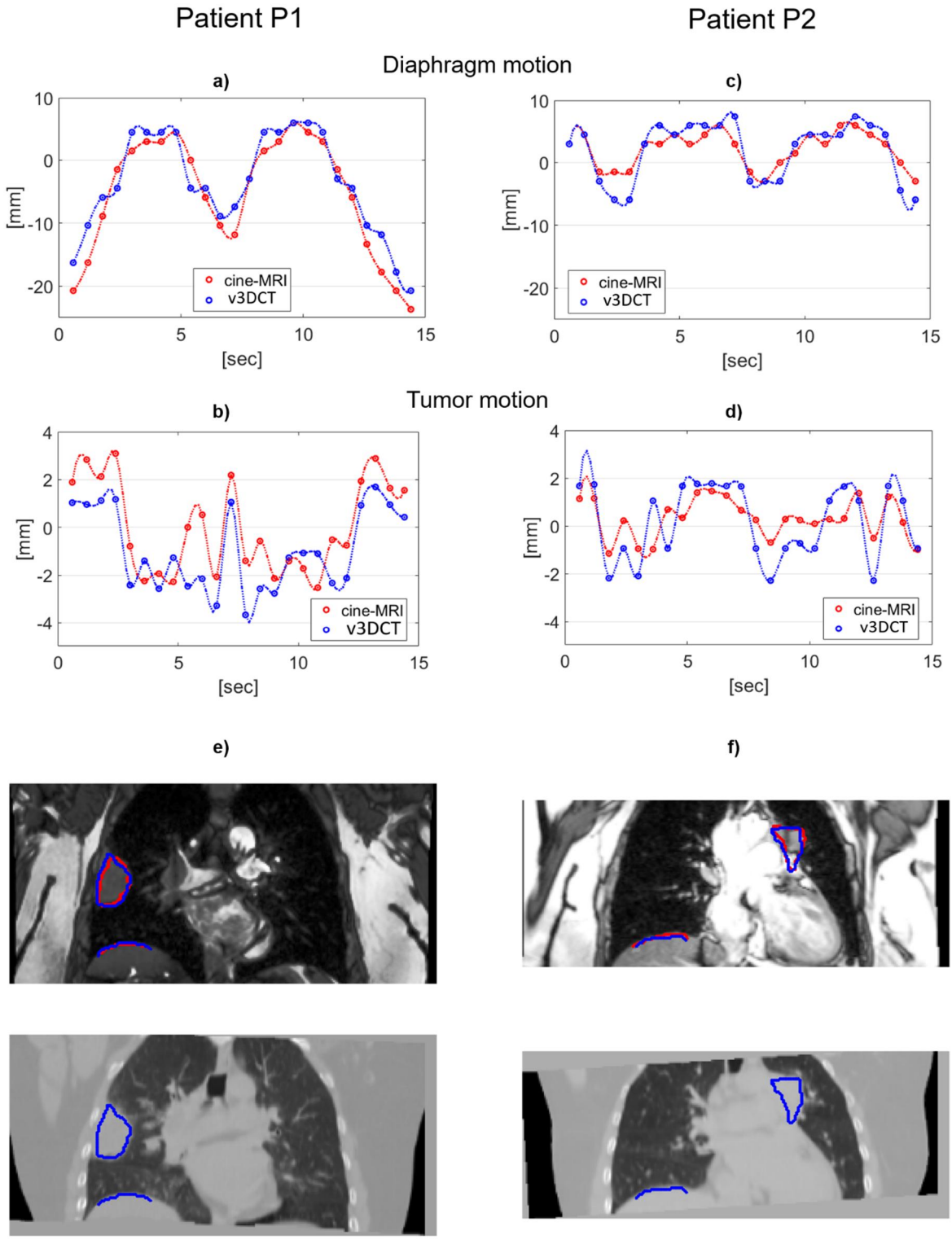

Figure 5. Diaphragm and tumor motion measured on cine-MRI data (red) and corresponding slices in v3DCT (blue). Panel a and b refers to patient P1 using the coronal plane. Contrarily, as both coronal and sagittal views were available for P2, panel c and d depict motion using both planes. Motion is reported in the SI direction. Panel e and f shows cine-MRI and v3DCT slices for P1 and P2, respectively. Also, contours of diaphragm profile and target volume for v3DCT (in blue) and cine-MRI (red) are shown.

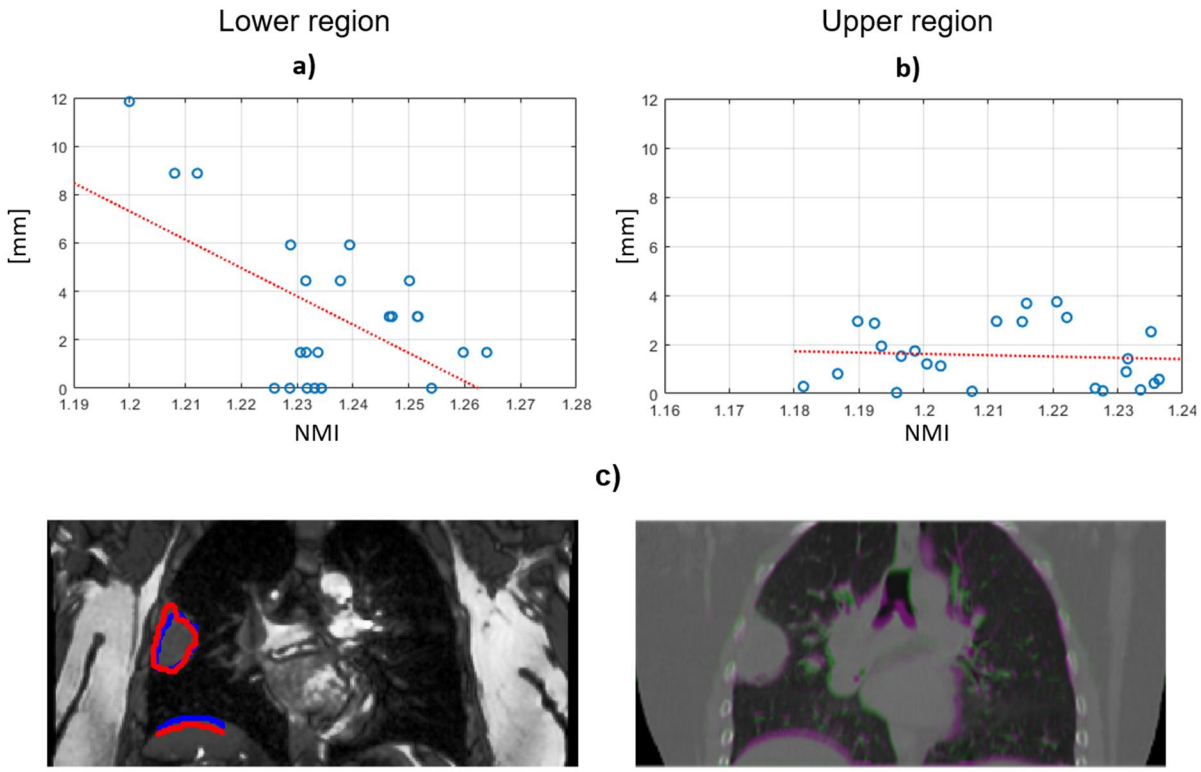

Figure 6. Comparison of estimated v3DCT and corresponding 4DCT phases for P1. Correlation between distances of associated respiratory phases and NMI in a) lower region (diaphragm-region) and b) upper region (tumor-region). Panel c) shows a qualitative comparison between the planning 3DCT-0% and a sample in the corresponding respiratory phase: contours distances are reported on the left (red = average-cycle sample; blue = in-room sample), while volume overlap on the right (green = average-cycle sample; violet = in-room sample).

3.3. Computational cost

Table 5 reports the computational cost of each step of the proposed workflow, to evaluate the potential use in a clinical environment. For the model construction during planning a total time of approximately 10min is required to perform mono-modal DIR and model construction. For model application during treatment, in-beam 2D multi-modal registration took about 20s, whereas 3s and 40s were needed for 3DVF estimation and CT reconstruction (inversion of the 3DVF included), respectively. Measurements were carried out on a general-purpose machine equipped with Intel® Xeon® processor (3.7 GHz) and 12GB RAM.

Table 5. Computational cost of the proposed ROI-based motion model.

Model construction		**Model application**	
3D DIR mono-modal (mean cycle)	**2D DIR mono-modal (mean cycle)**	**2D DIR multi-modal**	
447 s (for the entire cycle)	113 s (for the entire cycle)	18.35 s (for each sample)	
Model generation		**3D VF estimation**	**Volume reconstruction**
52 s		3.25 s (for each sample)	41.7 s (for each sample)

4. Discussion

A novel ROI-based motion model was proposed, featuring regional adaptation and estimation of in-room virtual CT volumes in an MRI-guided scenario for lung

treatments. The method was validated on a digital CT/MRI phantom and then applied to two lung patient cases.

4.1. ROI-based motion model

The first feature of the proposed model relies on the use of ROIs to account for irregular and uncorrelated motion between different anatomical structures (e.g. tumor motion vs. diaphragm motion). In the manuscript the method is presented considering a partition of the whole anatomy in two ROIs. This decision was determined after a preliminary analysis (supplementary materials B), which considered a different number of ROIs. The analysis highlighted the better performance of using two ROIs in the cranio-caudal direction (upper and lower region) that were described by specific anatomical structures (i.e. derived from tumor and diaphragm contour masks), than using different ROIs which do not rely on anatomical contours.

The accuracy of the mono-modal and multi-modal registration and the performance of the model were addressed in both phantom and patient's data, attesting the capability of the ROI-based model to accurately account for motion. As a result, an improved description of the patient entire anatomy during treatment is potentially available. Nonetheless, the considered ROIs were limited to regions described by tumor and diaphragm motion. In the future we plan to integrate the information stemming from other anatomical structures contoured on the planning 4DCT.

One limitation of the proposed model consists in reducing the information provided by the 2DVFs to their maximum/minimum values. This was due to the current implementation of the motion model, which reduced the motion information to their principal components. Future developments will consider (i) deriving the most informative subset of VF values rather than only maximum/minimum and (ii) improving the motion model to account for the whole 2DVF.

A further improvement of the motion model could also be represented by combining the ROIs definition with a separated description of the motion along the three anatomical directions (i.e. RL, AP and SI). This will potentially mitigate the detrimental effect of off-axis organ motion, as observed in patient P2 for the RL component.

Despite the limitations related to model construction, the proposed approach presents an innovative feature in the estimation of time-resolved virtual 3DCT volumes describing the patient anatomy during treatment. To our knowledge, this is the first motion model directly built on 4DCT and cine-MRI data of the lung. Current approaches rely on the acquisition of pre-beam 4DMRI and in-beam cine-MRI data of kidney and liver, with dosimetric evaluation derived on simulated pseudo-CT (Stemkens *et al.* 2017). On the contrary, the construction of our model within a multi-modal imaging pipeline including CT and MRI/cine-MRI data results in a CT-based anatomical characterization and, as such, suitable for dosimetric evaluation. Although the proposed approach is not currently implemented in real-time, it can be adopted retrospectively within a standard clinical workflow. Its use would allow one to evaluate the geometric accuracy of motion compensation strategies in current MRI-linac systems. In addition, the dosimetric accuracy of the delivered dose could be directly compared with the one planned on the 4DCT by means of dose accumulation, thus potentially achieving a closed-loop adaptive radiotherapy workflow (Paganelli *et al*. 2018).

However, a limitation of the current workflow relies on not including inter-fraction motion. Indeed, we assumed that no deformation occurred between 4DCT and MRI acquisition. Currently, a rigid registration is performed between 3DCT-0% and 3DMRI-0% since patient data present a breath-hold 3DMRI, which is not representative of the

free-breathing condition of the 4DCT. Future developments aim at including a pre-beam free-breathing 3D or, ideally, a 4DMRI acquisition in the proposed workflow (Stemkens *et al.* 2018). The availability of a 4DMRI will enable out-of-plane motion detection, not recognizable in cine-MRI, as well as a better evaluation of inter-fraction motion among respiratory phases. The inter-fraction motion can then be used to update the model built on the 4DCT, as proposed in Fassi *et al.* (2015). Despite this limitation, our results are within the maximum voxel dimension, attesting that the model is, at the current stage of development, able to compensate for motion. In addition, the proposed method effectively manages breathing motion baseline drifts that may occur during treatment. This is achieved by the selection of the maximum/minimum value of the 2DVF, according to on-line variations with respect to the 0% planning phase.
Moreover, the 2D DIR between the cine-MRI and sliceMRI-0% was included as supportive strategy for the multi-modal step. We also decided to include the T1-weighted MRI in the workflow since T1-weighted 4DMRI should be integrated into commercial scanners in the near future (Winkelmann *et al.* 2007; Deng *et al.* 2016). This will allow to acquire a 4DMRI with reduced respiratory artefacts, which will be included in the proposed workflow as pre-beam imaging. Finally, the method can be easily extended to a fully MRI-guided treatment, where no 4DCT is acquired and the model built on a 4DMRI.

4.2. Phantom study

For the phantom study, the ROI-based motion model performance was validated and compared against a conventional strategy proposed in the literature (Fayad *et al.* 2012) relying on a single motion trace (e.g. tumor or diaphragm motion alone). Although significant difference was not observed on the local tumor region, an improved organ motion compensation on both tumor and diaphragm can be appreciated. The conventional approach can mitigate errors effectively on the region in which it acts but lower performance is observed on other anatomical structures as shown by reported median errors (section 3.1).

In addition, as current MRI-linac systems feature both single (Mutic and Dempsey 2014) or interleaved (Langendijk *et al.* 2014) cine-MRI imaging capabilities, the method reliability was tested against different anatomical planes: coronal, sagittal and a combination of the two. Median errors below 1.45 mm were measured regardless the adopted plane. However, interleaved sagittal/coronal cine-MRI acquisition is expected to provide improved description of organ motion with respect to single plane imaging. The phantom validation confirmed this assumption, as a better motion description by the model was retrieved using interleaved cine-MRI images.

The availability of the phantom also allowed to compare the estimated motion field with the ground truth deformation, in order to evaluate the combination of the different VFs depending on the defined ROIs. Even if discontinuities were visible at the VFs interface (Figure 4), they do not affect image reconstruction, and maximum differences with respect to the ground truth motion were within 2mm. Larger errors were visible in the heart area mainly. This error does not have an impact on the performance of the ROI-based model since such differences were quantified also for the Fayad model, and a specific ROI defined on the heart could potentially mitigate it. Nevertheless, further investigations will include regularization methods to avoid discontinuities in the combination of VFs.

4.3. Patient study

For both lung patients, the ROI-based motion model was accurate in estimating tumor and diaphragm position, especially in the SI direction. For patient P1, errors below 2mm (i.e. maximum CT voxel resolution) were measured, attesting the ROI-based model capability to compensate for motion even when a single slice was available. As regards patient P2, the cine-MRI field of view limited the analysis of diaphragm motion to the coronal direction, where an error of 1.5mm for coronal/sagittal combination was found. Similarly, median tumor errors were below 1.5mm for the SI and AP component with the coronal/sagittal update planes. However, higher errors were quantified in the RL direction, an effect probably due to the tumor proximity to the heart which significantly affected motion.

Additionally, a 3D comparison was performed between the estimated volume and the correspondent respiratory phase of the planning 4DCT data. Even if this could not be considered a validation of the proposed approach, a correlation in the lower region was observed between the global measure and discrepancies between the associated respiratory phase, attesting that the model is producing physically sensible results. The lack of a significant correlation in the upper region was probably due to a tighter motion of the upper thorax with respect to the diaphragm motion.

Overall, the proposed method performed better than the conventional approach implemented in Fayad *et al.* (2012), showing its capability to account for motion regionally. Although the method was tested on in-room samples which differed from the planning condition, further investigations will be performed to evaluate the capability of the motion model to account for more irregular breathing patterns, baseline shifts as well as long term variations. A larger patient cohort is therefore required for a more comprehensive evaluation.

5. Conclusion

A novel ROI-based motion model technique has been developed and proposed as an integrating part of an envisioned clinical workflow based on 4DCT data and in-room MRI acquisition. Preliminary studies on a digital CT/MRI phantom and two lung cancer patients showed the feasibility of the proposed method. An extended clinical validation is foreseen to properly evaluate the method as a tool for accurate patient breathing motion estimation with dosimetric quantification capabilities.

Acknowledgments

This project is supported by the Australian National Health and Medical Research Council Program Grant APP1132471, Australia.

References

Bjerre T, Crijns S, Rosenschöld PM. "Three-dimensional MRIlinac intra-fraction guidance using multiple orthogonal cine-MRI planes." Phys. Med. Biol. 58:4943-4950, 2013.

Cervino LI, Jiang D, and Jiang SB. "MRI-guided tumor tracking in lung cancer radiotherapy." Phys. Med. Biol. 56: 3773-3785, 2011.

Colvill E, Booth J, Nill S, et al. "A dosimetric comparison of real-time adaptive and non-adaptive radiotherapy: A multi-institutional study encompassing robotic, gimbaled, multileaf collimator and couch tracking." Radiother Oncol;119:159–65, 2016.

Deng Z, Pang J, Yang W, et al. "Fourdimensional MRI using three-dimensional radial sampling with respiratory self-gating to characterize temporal phase-resolved respiratory motion in the abdomen." Magn. Reson.Med., 75: 1574–1585, 2016.
Fallone BG. "The rotating biplanar linac-magnetic resonance imaging system". Seminars in Radiation Oncology. 24: 200-202. 2014.
Fassi A, Seregni M, Riboldi M, et al. "Surrogate-driven deformable motion model for organ motion tracking in particle radiation therapy", Physics in Medicine & Biology. 60(4):1565-82, 2015.
Fast MF, Eiben B, Menten MJ et al. "Tumour auto-contouring on 2d cine MRI for locally advanced lung cancer: A comparative study." Radiother Oncol,125(3):485-491, 2017.
H. Fayad, J.F. Clement, T. Pan, C. Roux, C. Cheze I.e Rest, O. Pradier and O. Visvikis Towards a Generic Respiratory Motion Model for 40 CT Imaging of the Thorax IEEE Nuc!. Sci. Symp. Conf. Rec. 2009 , Page(s): 3975 – 3979
Fayad H, Buerger C, Tsoumpas C, et al. " A GenericRespiratory Motion Model Based on 4D MRI Imaging and 2D Image Navigators". IEEE NSS/MIC. 4058-4061. 2012.
Harris W, Lei R and Chang Z. "A Technique for Generating Volumetric Cine-Magnetic Resonance Imaging." Radiation Oncol Biol Phys, Vol. 95, No. 2, pp. 844e853,, 2016.
Hu, Y., S. D. Caruthers, D. A. Low, P. J. Parikh and S. Mutic. "Respiratory amplitude guided 4-dimensional magnetic resonance imaging." International Journal of Radiation Oncology* Biology* Physics 86(1): 198-204, 2013.
Jaffray D, Carlone MC, Milosevic MF, et al. "A Facility for Magnetic Resonance–Guided Radiation Therapy". Seminars in Radiation Oncology. 24: 193-195. 2014.
Jaffray DA. "Image-guided radiotherapy: from current concept to future perspectives." Nat. Rev. Clin. Oncol. 9, 688–699, November 2012.
Kamerling CP, Fast MF, Ziegenhein P, et al. "Real-time 4D dose reconstruction for tracked dynamic MLC deliveries for lung SBRT." Med Phys ;43(11):6072–81, 2016.
Keall, PJ, GS Mageras, JM Balter, et al. "The Management of Respiratory Motion in Radiation Oncology." Med Phys. 33:3874-3900, 2006.
Keall P. "4-Dimensional Computed Tomography Imaging and Treatment Planning." Seminars in Radiation Oncology. 14:81-90, 2004.
Keall P, Barton M, Crozier S."The Australian magnetic resonance imaging-linac program". Seminars in Radiation Oncology. 24: 203-206. 2014.
Langendijck JJW, Raaymakers BW, and van Vulpen M. "The magnetic resonance imaging-linac system." Seminars in Radiation Oncology. 24:207-209, 2014.
Lee D, Greer PB, Ludbrook J, Arm J, and Hunter P. "Audiovisual Biofeedback Improves Cine–Magnetic Resonance Imaging Measured Lung Tumor Motion Consistency." Int J Radiat Oncol Biol Phys., 94(3):628-36, 2016.
Mazur TR, Fischer-Valuck BW, and Wang Y. "SIFT-based dense pixel tracking on 0.35 T cine-MR images acquired during image-guided radiation therapy with application to gating optimization." Med Phys; 43(1):279, 2016.
McClelland JR, Hawkes DJ, Schaeffter T, and King AP. "Respiratory motion models: A review." Medical Image Analysis 17, 2013.
Menard C, and U van der Heide. "Introduction: Systems for Magnetic Resonance Image Guided Radiation Therapy." Seminars in Radiation Oncology 24, 2014.

Menten MJ, Wetscherek A, Fast MF, et al. "MRI-guided lung SBRT: Present and future developments." Phys Med. (in press), 2017.

Mutic S and Dempsey JF. "The ViewRay System: Magnetic Resonance – Guided and Controlled Radiotherapy." Seminars in Radiation Oncology. 24: 196-199, 2014.

Paganelli, C., P. Summers, M. Bellomi, G. Baroni and M. Riboldi. "Liver 4DMRI: A retrospective image-based sorting method." Medical physics 42(8): 4814-4821, 2015.

Paganelli C, Greer PG, Baroni G, Riboldi M, and Keall P. "Quantification of lung tumor rotation with automated landmark extraction using orthogonal cine-MRI images." Physics in Medicine and Biology, 60: 7165-7178, 2015.

Paganelli C, Summers P, Gianoli C, Bellomi M, Baroni G, and Riboldi M. "A tool for validating MRI-guided strategies: a digital breathing CT/MRI phantom of the abdominal site" Medical and Biological Engineering and Computing; 55(11):2001-2014, 2017.

Paganelli C, Whelan B, Peroni M, Summers P, et al. MRI-guidance for motion management in external beam radiotherapy: current status and future challenges. Phys Med Biol, https://doi.org/10.1088/1361-6560/aaebcf, 2018.

Park JM, Park SY, Kim HJ, et al. "A comparative planning study for lung SABR between tri-Co-60 magnetic resonance image guided radiation therapy system and volumetric modulated arc therapy." Radiother Oncol;120(2):279-85, 2016.

Sawant A, Keall P, Pauly KB, et al. "Investigating the Feasibility of Rapid MRI for Image-Guided Motion Management in Lung Cancer Radiotherapy." BioMed Res Int. 485067, 2014.

de Senneville B.D., Hamidi A.El, and Moonen C. "A Direct PCA-Based Approach for Real-Time Description of Physiological Organ Deformations." IEEE Trans Med Imaging. 34(4): 974-982, 2015.

Seregni M, Paganelli C, Lee D, et al. "Motion prediction in MRI-guided radiotherapy based on interleaved orthogonal cine-MRI." Phys Med Biol ;61:872–87, 2016.

Seregni M, Paganelli C, Summers P, Bellomi M, Baroni G, and Riboldi M. "A Hybrid Image Registration and Matching Framework for Real-Time Motion Tracking in MRI-Guided Radiotherapy." IEEE Trans Biomed Eng. 65(1):131-139, 2018.

Shi X, Diwanji T, Mooney KE, et al. "Evaluation of template matching for tumor motion management with cine MR images in lung cancer patients." Med Phys. 41: 052304, 2014.

Stemkens B, Glitzner M, Kontaxis C, et al. "Effect of intra-fraction motion on the accumulated dose for free-breathing MR-guided stereotactic body radiation therapy of renal-cell carcinoma." Phys Med Biol ;62(18):7407-7424, 2017.

Stemkens B, Tijssen RHN, de Senneville BD, Langendijk JJW, and van den Berg CAT. "Image-driven, model-based 3D abdominal motion estimation for MR-guided radiotherapy." Phys. Med. Biol. 61: 5335, 2016.

Stemkens B, Paulson ES, Tijssen RHN. Nuts and bolts of 4D-MRI for radiotherapy. Phys Med Biol, doi: 10.1088/1361-6560/aae56d. 2018.

Tong Y, Udupa JK, and Ciesielski KC. "Graph-based retrospective 4D image construction from free-breathing MRI slice acquisitions." Proc. SPIE. 9038: 90380I-1–90380I-7, 2014.

Tryggestad E, Flamming A, Hales R, et al. "4D tumor centroid tracking using orthogonal 2D dynamic MRI: Implications for radiotherapy planning." Med Phys. 40: 091712, 2013a.

Von Siebenthal, M., G. Székely, U. Gamper, P. Boesiger, A. Lomax and P. Cattin. "4D MR imaging of respiratory organ motion and its variability." Physics in medicine and biology 52(6): 1547, 2007.

Winkelmann S, Schaeffter T, Koehler T, and Eggers H "An optimal radial profile order based on the Golden Ratio for time-resolved MRI." IEEE Trans Med Imaging. , 2007: 26(1):68-76.

Wölfelschneider J, Seregni M, Fassi A, et al. "Examination of a deformable motion model for respiratory movements and 4D dose calculations using different driving surrogates." Med Phys. 44(6):2066-2076, 2017.